Research Article **Open Access**

Linbao Luo, Caiwang Ge, Yifei Tao, Lie Zhu, Kun Zheng, Wei Wang, Yongxuan Sun, Fei Shen, and Zhongyi Guo*

High-efficiency refractive index sensor based on the metallic nanoslit arrays with gain-assisted materials

DOI: 10.1515/nanoph-2016-0028
Received November 27, 2015; accepted February 23, 2016

Abstract: We have designed and investigated a three-band refractive index (RI) sensor in the range of 550–900 nm based on the metal nanoslit array with gain-assisted materials. The underlying mechanism of the three-band and enhanced characteristics of the metal nanoslit array with gain-assisted materials, have also been investigated theoretically and numerically. Three resonant peaks in transmission spectra are deemed to be in different plasmonic resonant modes in the metal nanoslit array, which leads to different responses for the plasmonic sensor. By embedding the structure into the CYTOP with proper gain-assisted materials, the sensing performances can be greatly enhanced due to a dramatic amplification of the extraordinary optical transmission (EOT) resonance by the gain medium. When the gain values reach their corresponding thresholds for the three plasmonic modes, the ultrahigh sensitivities in three bands can be obtained, and especially for the second resonant wavelength (λ_2), the FOM=128.1 and FOM*= 39100 can be attained at the gain threshold of k =0.011. Due to these unique features, the designing scheme of the proposed gain-assisted nanoslit sensor could provide a powerful approach to optimize the performance of EOT-based sensors and offer an excellent platform for biological sensing.

Keywords: Gain-assisted materials, nanoslit arrays, cavity mode, surface plasmon resonance (SPR)

***Corresponding Author: Zhongyi Guo:** School of Electronics Science and Applied Physics, Hefei University of Technology, Hefei, 230009, China
and School of Computer and Information, Hefei University of Technology, Hefei, 230009, China, E-mail: guozhongyi@hfut.edu.cn
Linbao Luo: School of Electronics Science and Applied Physics, Hefei University of Technology, Hefei, 230009, China, E-mail: luolb@hfut.edu.cn
Caiwang Ge: School of Electronics Science and Applied Physics, Hefei University of Technology, Hefei, 230009, China
and School of Computer and Information, Hefei University of Technology, Hefei, 230009, China
Kun Zheng: School of Electronics Science and Applied Physics, Hefei University of Technology, Hefei, 230009, China
Yifei Tao, Lie Zhu, Wei Wang, Yongxuan Sun, Fei Shen: School of Computer and Information, Hefei University of Technology, Hefei, 230009, China

1 Introduction

Ten years ago, optical transmission through periodic metal nanoscale film arrays [1], with intensity beyond the predicted by the standard theory [2], was called the extraordinary optical transmission (EOT). In recent years, extensive investigations about the EOT of subwavelength metallic structures have been implemented [3, 4], which have a great potential to control light and carry the promise of different applications in many areas, such as sensing [5], subwavelength optics [6], optoelectronics devices [7, 8], and so on. And many efforts have also been made to explain the unique phenomena of EOT, and the existence of the surface plasmon resonance (SPR) and cavity mode (CM) [9, 10] have been considered. The SPR and CM can be supported by various metal nano-array [11–13], and the resonant spectra of the SPR and CM sensitively vary with the geometric parameters and the environmental refractive index (RI) around the structures. Therefore, the properties of these EOT resonances induced by the SPR and CM can allow a label-free optical sensing.

Owing to the fact that the transmission spectra of the metal nano-array are sensitive to the RI changes, these EOT-based metal nano-array sensors have been widely discussed in the previous literature [14, 15]. Compared with traditional SPR sensor chip, the nano-array sensor can not only monitor the label-free analytes in real time but also significantly reduce the integration volumes and fabricating cost. However, the EOT-based sensors usually provide much lower sensitivity than the conventional SPR technique, so enhancing their performance is a significant focus of current research on plasmonics [16, 17]. Many researchers have developed and optimized some EOT-based sensors with different strategies, such as us-

ing suspended metal films [18], changing the shape of nano-patterns [19–21], employing more complex structures [22, 23]. However, in all of these studies, they suffer from a large intrinsic Ohmic loss in metal materials, which hinders further improvements of the performances (spectra intensity, quality factor, signal-to-noise ratio) of the EOT-based sensors. Recently, nonlinear active media such as dye molecules, quantum wells, or dots have been used to compensate for the Ohmic loss in plasmonic structures [24, 25]. The energy transfer from the gain media to the metal nanostructures not only compensates for the system loss, but also enhances the plasmonic resonance in several orders of magnitude accordingly in such active plasmonic systems. Many gain-assisted LSPR-based sensors have been studied, such as gold nanoparticles embedded in gain medium [26] and gain-assisted metal-silica core shell structure [27, 28]. In particular, a gain-assisted plasmonic analog of electromagnetically induced transparency (EIT) in a metallic metamaterial has also been investigated, and the transmittance spectrum intensity of the EIT-based sensor can be amplified by two orders of magnitude nearly and its sensitivity has also been enhanced greatly [29]. However, only a few studies have been done on the gain-assisted EOT-based sensors' performance in metal nano-array structures.

In this paper, we have demonstrated theoretically that the resonance amplification in active plasmonic structures can be applied to EOT-based sensors with a great enhancement of the sensing capability. We show that the EOT efficiency of the nanoslit array depends strongly on the Ohmic loss in the metal nanoslit array system, which hinders further to improve the performance of the EOT-based sensors. By embedding the structure into the CYTOP with proper gain-assisted materials, the confined optical field and transmittance intensity of the EOT system can be improved greatly. Meanwhile, the gain-assisted nanoslit array sensor has a ultrahigh sensitivity when the gain value reaches the corresponding thresholds for the three transmission spectra ($\lambda_1 - \lambda_3$), and the ultrahigh FOM=128.1 and FOM*= 39100 (for resonant wavelength of λ_2) can be obtained at the gain threshold of k =0.011. The demonstrated capability of the gain-assisted nanoslit array sensor opens up a new opportunity to optimize the performances of EOT-based sensors and holds potential applications in biomedical and environmental sensing.

2 Structure model and simulation method

The schematic structure of the used periodic metallic array of silver nanoslits is shown in Fig. 1. It has been demonstrated that the substrates with a lower index can further increase the EOT efficiency and improve the sensor performance [30, 31]. And the CYTOP is a highly transparent and chemically stable fluoropolymer with a low RI of n1 very close to that of water, so we consider the nanoslit array is embedded in CYTOP (with the RI of n1≈n_{water} =1.33) to match the RI of water environment above the structures. The period, width, and depth of the slit are indicated as P, W, and D, respectively. What's more, a cover layer of t =20 nm of CYTOP was added to protect the Ag nanoslits array from oxidation. The frequency-dependent permittivity of silver is described by Drude model: $\varepsilon_m(\omega) = \varepsilon_\infty - \omega_p^2/(\omega^2 - i\omega y)$ with the constants ε_∞ =3.8, ω_p =1.37 × 10^{16} rad s^{-1} and y =9.9140 × 10^{13} rad s^{-1} [32]. Here, ω is the angular frequency of the incident light. All results are calculated using the finite element method (FEM) and we set the periodic boundary conditions in both the x and y directions. The perfectly matching layers (PMLs) are utilized at the calculated region boundaries to reduce the influence of light reflection. The transverse magnetic (TM) polarized light is assumed to be normally incident from the top of the structure.

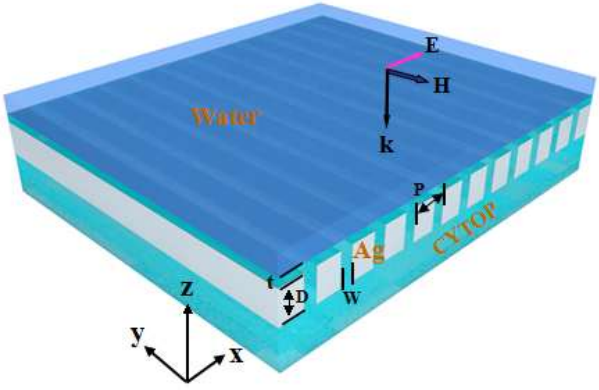

Fig. 1. Schematic of a metallic nanoslit arrays embedded in the CYTOP, with the geometrical parameters (t, D , W and P), and the direction of the TM-polarized incident light.

3 Results and discussion

3.1 EOT behavior in metal nanoslit array

Here, we set the parameters of the nanoslit array as follows: P =500 nm, D =460 nm, W =25 nm, t =20 nm. As depicted in Fig. 2(a), there are three resonant peaks in the transmittance spectrum, denoted as λ_1, λ_2, λ_3, respectively. To better understand the underlying mechanisms of the three transmittance peaks, the magnetic fields are extracted from the simulated resonant peaks, as shown in Figs. 2(b, c, d). In general, there will be the resonant modes in the transmission spectra, such as the cavity mode (CM) or the SPP modes by modulating the parameters properly (including the depth of the film and the period and the width of the nanoslits). When the depth of the deposited mental film is large enough, there will exist multiorder CMs in the transmission spectra, which can be marked as CMl respectively, and "l" denote the orders of the CM in the nanoslits, corresponding to the number of nodes in the magnetic field distributions [33]. Just as shown in Figs. 2(b) an 2(d), for the resonances at λ_1 =586 nm and λ_3 =792 nm, the main magnetic fields intensities are all confined between the slit walls and the number of nodes are l =3 and l =2, respectively, which corresponding to the third and second CMs, accordingly. At λ_2 =635 nm, the magnetic field is strongly confined in the slit walls and the interfaces of the metal–water, metal–CYTOP, which can be attributed to the couplings of CMs in nanoslits and excited SPP on the metal surfaces as confirmed by the associated field distributions in Fig. 2(c). Note that the existence of a propagating CM inside the slits also always couples the SPP modes at both metal surfaces.

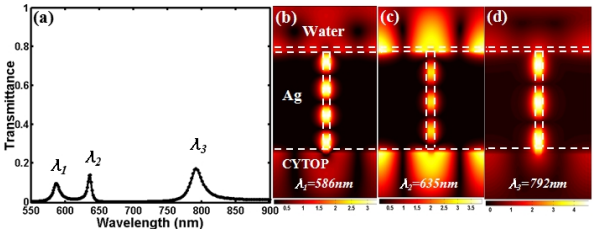

Fig. 2. Transmission spectrum of nanoslit arrays with P =500 nm, D =460 nm, W =25 nm, t =20 nm (a). Calculated magnetic field distributions at resonant peaks of λ_1 (b), and λ_2 (c), λ_3 (d), respectively. The white dotted lines mark the boundaries of the structure.

Figure 3(a) shows the influences of nanoslit period on the transmittance and the bandwidth of the nanoslit array. The resonant peaks of λ_1 and λ_3 have slight red shift and the full width at half maximum (FWHM) become narrower with increasing the nanoslit periods, while the resonant peak of λ_2 has an obvious red shift and its FWHM has been broadened slightly with increasing nanoslit periods. The larger red-shift of the λ_2 is due to the array period directly impacts the SPP mode according to the following equation [22]:

$$\lambda_{spp}(n,i) = \frac{P}{i} Re\left\{\left(\frac{\varepsilon_m n^2}{\varepsilon_m + n^2}\right)^{1/2}\right\} \quad (1)$$

where n is the RI of environmental materials, i denotes the resonant order (i =1 in this paper), P is the period of the nanoslit arrays and ε_m is the dielectric constant of the metal. Evidently, the equation shows the SPP's resonant wavelength is sensitive to the variation of the nanoslit period and environmental RI, which indicated that the nanoslit array can be used as SPP based sensors by properly tuning the period of P. Furthermore, as we all know that the CMs mainly affected by the metal film depth [22, 34], so we calculated the influences of metal film depth on the transmission spectra as shown in Fig. 3(b). As the nanoslit depth increase from 420 to 520 nm, the resonant CMs of λ_1 and λ_3 gradually shift to longer wavelengths, and the peak intensities and the bandwidth also increase accordingly. Whereas the coupling SPP mode of λ_2 just demonstrate a slight red shift and its FWHM becomes narrower slightly. These characteristics of the transmission peaks induced by different plasmonic modes and geometric parameters can lead to different responses for the plasmonic sensors.

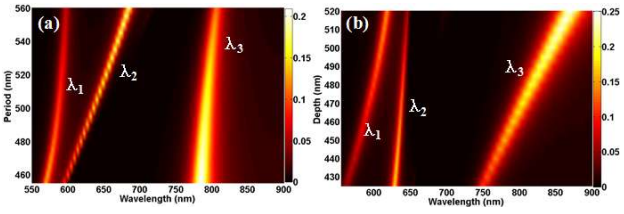

Fig. 3. Transmission intensities through a nanoslit array as a function of wavelength (λ) and slit period (a), wavelength (λ) and slit depth (b).

3.2 Functions of the gain-assisted medium

However, the FWHM of the resonant peaks at λ_1, λ_2, and λ_3 are 12.2, 7, and 20 nm, respectively, and the maximum transmission intensity "I" for $\lambda_1 - \lambda_3$ can only reach to 0.17. The broad bandwidth and weak transmission intensity are

harmful for the sensing performances, and these problems may originate from the intrinsic Ohmic loss in metal nanoslit arrays. To demonstrate the underlying physics behind the Ohmic loss effect, we calculate the transmission spectra of a silver nanoslit array as a function of absorption factor of $0 \le f_{abs} \le 1$ that controls the amount of Ohmic absorption in Ag with its dielectric constant $\varepsilon_M = \varepsilon_M + i * f_{abs} * \varepsilon_M$. In experiments, f_{abs} can be adjusted by tuning temperatures, such as f_{abs} =1 at room temperature and f_{abs}<1 in the lower temperature range. Fig. 4 shows the results for f_{abs} =0.2, 0.4,0.6, 0.8, and 1, from which we can observe that the FWHM become smaller and transmission intensity "I" becomes stronger with decreasing f_{abs}. For example, we obtain FWHM=7, 5, and 12 nm and I =0.39, 0.54, 0.60 for $\lambda_1 - \lambda_3$ at f_{abs} =0.2, respectively. So we can make sure that the limitations (the broad bandwidth and weak transmission intensity) are originating from the intrinsic Ohmic loss of metal system mainly, which hinders the improvements of the EOT efficiencies and the EOT-based sensor performances.

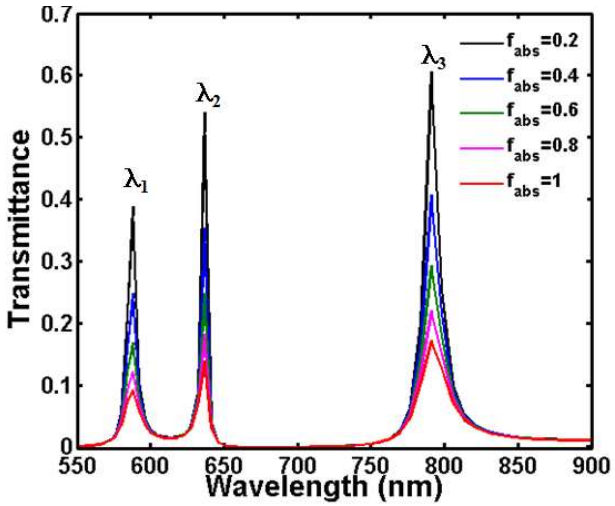

Fig. 4. Transmission spectra of silver nanoslit array with different metal absorption factors of f_{abs}.

Recently, nonlinear active media such as quantum wells or dots and dye molecules have been used to compensate for the Ohmic loss in plasmonic structures [24, 25]. Here, we consider that the metal nanoslit array imbedded in a host dielectric (CYTOP) with optical gain material. The gain-assisted dielectric material is described by a complex reflective index as n =1.33 – ki, where gain efficiency of k adjusts the amount of optical gain. To understand the microscopic details of the gain-assisted nanoslit array, we can describe the interactions between the electromagnetic fields and the active gain medium by using a four-level quantum system as shown in Fig. 5(a). The four-level system is initially assumed to be in the ground level |0>, and the incident photons induce an electronic transition from the ground level |0> to the highest level |3>. After a fast nonradiative transition from the highest level |3> to the upper level |2>, the excited gain system returns to level |1> either by radiating photons or by transferring its energy to the silver nanoslit array. In other words, the gain medium transfers its energy to the EOT resonance of the nanoslit array by interaction between the EM fields and gain medium. As shown in Fig. 5(b), we calculate the transmission spectra of the gain-assisted nanoslit array at different levels of the gain by setting different gain values of k. It is found that the transmission intensity of the resonant peaks (λ_1, λ_2, and λ_3) have different variations with different optical gains (k). That is to say, there has been an energy matching among the gain, the incident light, and the EOT resonance of the slit-array system. At a proper gain value, a "super" resonance will be achieved with the transmission reaching its maximum, and this gain value can be called the "threshold" accordingly that can be used to build up the strong amplification of the EOT resonance [35].

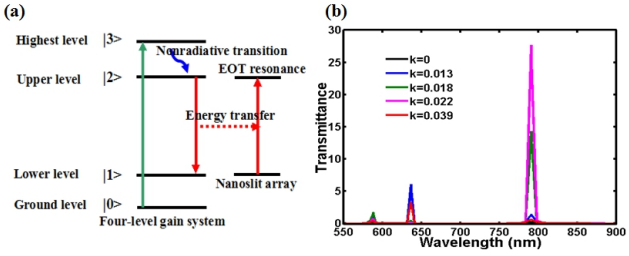

Fig. 5. (a) Schematic of the energy transfer from an optically excited four-level gain medium to the EOT resonance of the nanoslit array. (b) The transmission spectra of nanoslit array with different values of optical gain.

To investigate the corresponding thresholds for the resonant peaks of $\lambda_1 - \lambda_3$, calculated results about transmission spectra and magnetic field distributions of $\lambda_1 - \lambda_3$ with different gain values are presented in Figs. 6(a)-6(c), respectively. With increasing k, the transmittance increase to more than 1, which means that the gain medium is sufficient to compensate the system loss and the nanoslit array start to operate as an optical amplifier. When k further increased to the threshold, the amplification and the system loss reach a dynamical balance with the transmittance reaching a maximum value. As shown in Figs. 6(a)–6(c), the threshold for the resonant peaks of $\lambda_1 - \lambda_3$ are k = 0.017, 0.011, 0.02, respectively. And a level with near four orders of amplification in transmittance intensity can

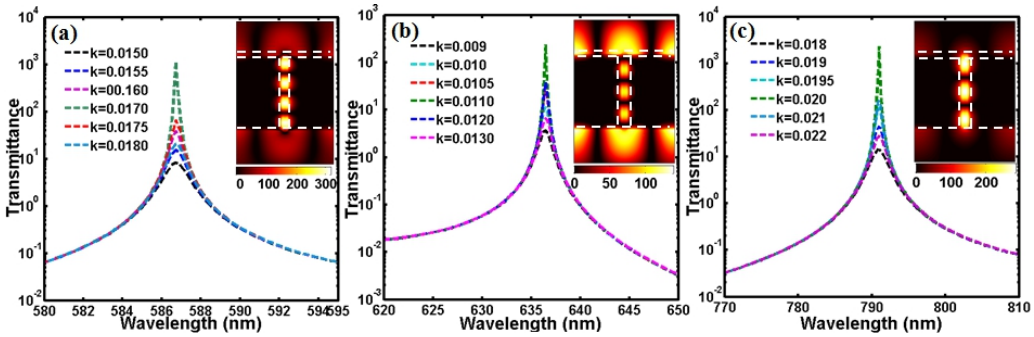

Fig. 6. Transmittance spectra of different gain values assisted nanoslit array for $\lambda_1 - \lambda_3$, respectively. The inset in (a)–(c) show the enhanced magnetic field distributions of the structure at corresponding gain threshold for $\lambda_1 - \lambda_3$.

reach at corresponding thresholds for the resonant peaks of λ_1–λ_3. For example, the value of "I" can reach 1163 at the threshold of k =0.02, while that for the same nanoslit array but with no optical gain (k =0) is just 0.1 . Meanwhile, the magnetic field intensities have also been enhanced around two orders of magnitude at corresponding thresholds compared with that with k =0 for the resonant peaks of $\lambda_1 - \lambda_3$, as shown in the inset of Figs. 6(a)-6(c). Moreover, we can obtain an extremely narrow bandwidth (FWHM) below 1 nm at corresponding threshold of $\lambda_1 - \lambda_3$. These will greatly enhance the performances of the gain-assisted nanoslit array for sensing applications.

3.3 Gain-assisted nanoslit array for sensing applications

To study the performances of the gain-assisted nanoslit array sensor, we have calculated the transmission spectra (Figs. 7(a)–(c)) under normal excitation when the structure (with gain value equal to the corresponding thresholds) is immersed in a series of sodium chloride–water mixture solutions with varying concentrations of 0%, 5%, 12%, and 20% with the corresponding RIs of 1.33, 1.34, 1.35, and 1.36, respectively [26]. Obviously, a rather small change in the RI of the solution can result in an apparent change in transmission spectra. The spectral positions of these resonances versus the RIs are plotted in Figs. 7(d–f), respectively, and the RI sensitivities (S= $\partial\lambda$(nm)/∂n(RIU)) of 33.33, 102.5, and 47.17 nm/RIU are obtained by linear fittings for the resonant peaks of λ_1 – λ_3 accordingly. The FWHMs are around 0.6, 0.8, and 0.5nm corresponding to the resonant peaks of $\lambda_1 - \lambda_3$. Therefore, the figure of merit (FOM=S(nm RIU-1)/FWHM(nm)) for the resonant peaks of λ_1 – λ_3 can be obtained as 55.5, 128.1, and 94.34, respectively [36]. Significantly, the resonant peak of λ_2 has a higher sensitivity than that of λ_1 and λ_3, which can be attributed as the change of the top surface from water–metal to solutions–metal, where the generated SPP will be affected directly. The high sensitivity to the environmental RI changes of the nanoslit array indicate that the designed structures have a great potential in optical sensing.

It should be noted that the sensitivities (S) of all resonant peaks (λ_1~λ_3) have a relatively low value. The maximum of them is around 102.5 nm/RIU for the resonant wavelength λ_2. First, the resonance peak (λ_2) should be attributed to the couplings of CMs in nanoslits and excited SPP on the interfaces of the metal–water, metal–CYTOP (confirmed by the associated field distributions in Fig. 2(c)). But the detection object (sodium chloride–water mixture solution) only cover on the top surface (the interfaces of the metal–water), because of the surface tension of the liquid. So the sensitivity may not be very large. On the other hand, the lower sensitivity is also influenced by the upper 20 nm layer CYTOP. Figure 8 demonstrates the sensitivity as a function of the CYTOP's thickness. Evidently, the thinner CYTOP is, the larger sensitivity will be obtained. The sensitivity can reach 165nm/RIU if there is no CYTOP covered on the top surface. Even so, the value of sensitivity remains relatively low.

In real experiments, it is much more convenient to monitor the changes in spectrum intensity at a fixed wavelength instead of the peak/dip shifts induced by changes in RI of the surrounding medium. Therefore, an alternative figure of merit, termed FOM*, was proposed for evaluating the sensor's performances [37], which is defined as:

$$\mathrm{FOM}^{*} = \max\left|\frac{\mathrm{d}I(\lambda)/\mathrm{d}n(\lambda)}{I(\lambda)}\right| \qquad (2)$$

where d$I(\lambda)$/I(λ) is the relative intensity change at a fixed wavelength λ induced by an RI change of dn. FOM* is not associated with the FWHM directly, which is better for evaluating the intrinsic sensing ability of the RI sensors. Figures 7(a–c) present the FOM* in the resonant peaks of λ_1 – λ_3 as a function of wavelength at different RIs of

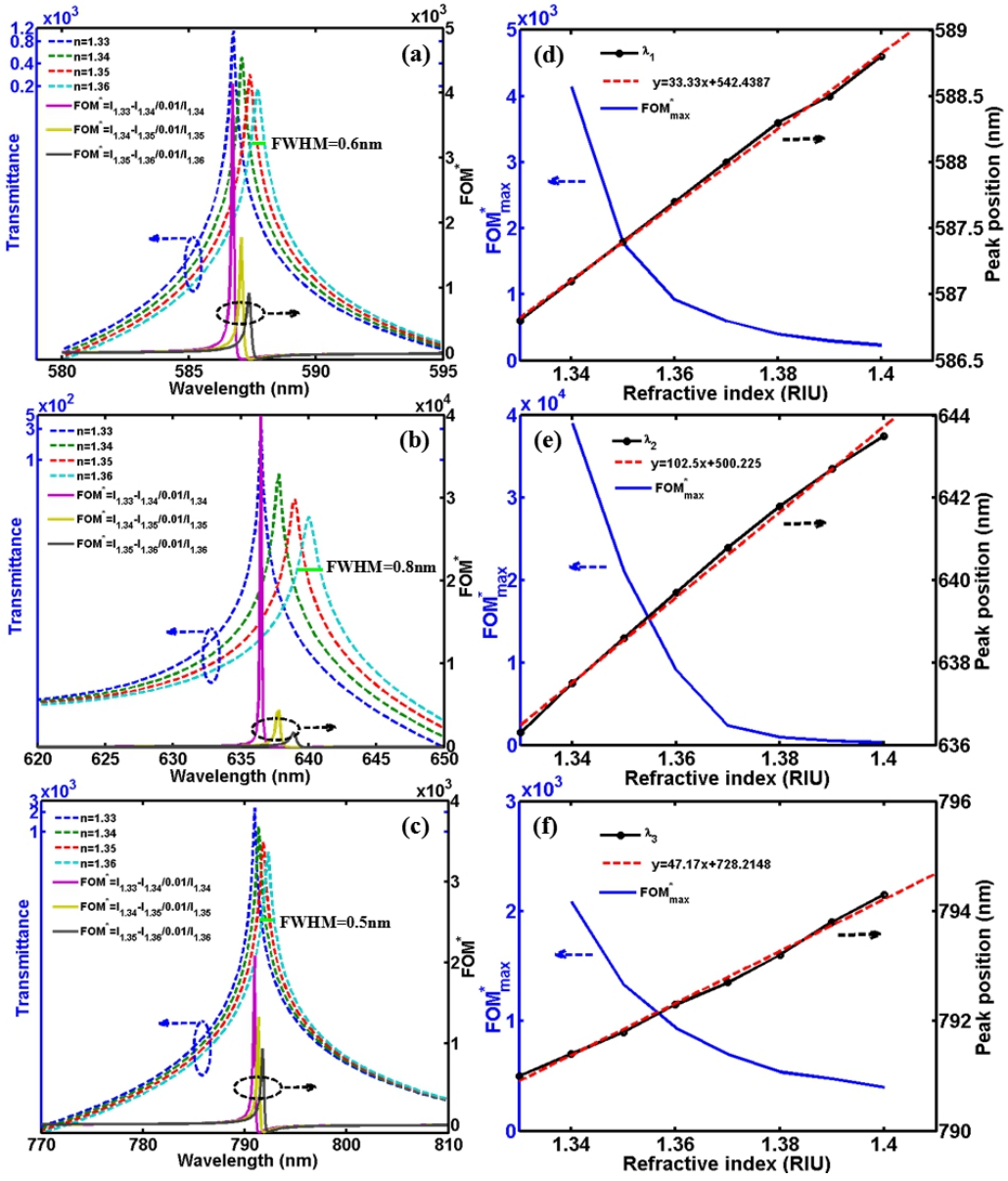

Fig. 7. (a)–(c) Transmission spectra and FOM* of the resonant peaks (λ_1 – λ_3) when the structure is immersed in sodium chloride–water mixture solutions with varying concentrations. (d)–(f) The FOM*max and peak positions for the resonant peaks (λ_1 – λ_3) as a function of the varying RI, respectively.

chloride–water solutions. The maximum value of FOM* (FOM*$_{max}$) are around 4140, 39100, and 2086 nm for the resonant peaks of λ_1 – λ_3 and they all occur at the corresponding resonant peaks. These values of FOM* have been improved by at least two orders of magnitude compared with that in previous literature [37]. It is noteworthy that the FOM* will be decreasing with increasing the RI of the surrounding medium as shown in Figs. 7(a~c). For clarity, we have calculated the FOM*$_{max}$ at different concentrations of chloride–water solutions (RI changing from 1.33 to 1.40), for the resonant peaks of λ_1 – λ_3, as shown in Figs. 7(d–f) respectively. We can observe that the FOM*$_{max}$ dropped rapidly with increasing the RIs of surrounding mediums, which can be attributed as the mismatch among the gain, the incident light, and the EOT resonance of the nanoslit array. In other words, the thresholds for the resonant peaks of $\lambda_1 - \lambda_3$ are changing with increasing RI, so the corresponding transmission intensity will decay with the mismatched thresholds. However, all of the minimum values of FOM*$_{max}$ for the resonant peaks of $\lambda_1 - \lambda_3$ are more than 200 at RI=1.40 (Figs. 7(d~f)), which demonstrate that the gain-assisted sensor has a higher

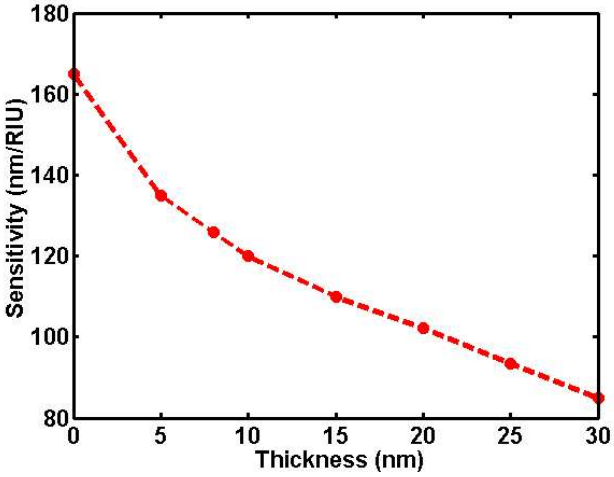

Fig. 8. The sensitivity as a function of the thickness of layer of the CYTOP.

sensitivity in a larger detecting range. The characterized wavelength in our work mainly focuses on the visible region, which is compatible with current data of the plasmon sensor [38, 39]. And these different responses at different resonance peaks will enhance the selectivity and the sensitivity of the sensors for the real sensing applications.

4 Conclusions

In summary, we have theoretically and numerically investigated the EOT effect and the sensing performance of the gain-assisted silver nanoslit array. We find that the intrinsic Ohmic loss of system hinders the improvement of the EOT efficiency of the nanoslit array. To compensate for the intrinsic loss, we propose a method by embedding the structure in the gain-assisted medium . When the gain value reaches its corresponding threshold, both the magnetic field and transmission intensity can reach a ultrahigh value because of the amplified EOT resonance by the energy transferred from the gain. Meanwhile, the gain-assisted nanoslit sensor also has an ultrahigh enhancement of the sensing performance, for example, the FOM and FOM* (for resonance wavelength λ_2) can reach to 128.1 and 39100, respectively. The gain-assisted nanoslit array with the ultrahigh sensitivity to the RI changes of surrounding medium will be found broad applications in biomedical and environmental sensing.

Acknowledgment: The authors gratefully acknowledge the financial support for this work from the National Natural Science Foundation of China under Grant No. 61575060, and the Fundamental Research Funds for the Central Universities (2015HGCH0010).

References

[1] T. W. Ebbesen, H. J. Lezec, H. F. Ghaemi, T. Thio, and P. A. Wolff, Extraordinary optical transmission through sub-wavelength hole arrays, Nature 391 (1998) 667-669.
[2] R. Gordon, Bethe's aperture theory for arrays, Phys. Rev. A 76 (2007) 053806.
[3] F. J. García-Vidal, L. Martín-Moreno, T. W. Ebbesen, and L. Kuipers, Light passing through subwavelength apertures, Rev. Mod. Phys. 82 (2010) 729-787.
[4] M. M. Alkaisi, R. J. Blaikie, S. J. McNab, R. Cheung, and D. R. S. Cumming, Subdiffraction-limited patterning using evanescent near-field optical lithography, Appl. Phys. Lett. 75 (1999) 3560–3562.
[5] C. Genet, and T. W. Ebbesen, Light in tiny holes, Nature 445 (2007) 39–46.
[6] X. G. Luo, and T. Ishihara, Sub-100-nm photolithography based on plasmon resonance, Jap. J. Appl. Phys. 43 (2004) 4017–4021.
[7] S. Collin, F. Pardo, and J. L. Pelouard, Resonant-cavity-enhanced subwavelength metal-semiconductor-metal photodetector, Appl. Phys. Lett. 83 (2003) 1521–1523.
[8] C. Liu, V. Kamaev, and Z. V. Vardeny, Efficiency enhancement of an organic light-emitting diode with a cathode forming two-dimensional periodic hole array, Appl. Phys. Lett. 86 (2005) 143501.
[9] S. Roh, T. Chung, B. Lee, Overview of the characteristics of micro-and nano-structured surface plasmon resonance sensors, Sensors 11 (2011) 1565-1588.
[10] C. Ge, Z. Guo, Y. Sun, F. Shen, Y. Tao, J. Zhang, R. Li and L. Luo, Spatial and spectral selective characteristics of the plasmonic sensing using metallic nanoslit arrays, Opt. Commun. 359 (2016) 393-398.
[11] J. Zhang, Z. Guo, C. Ge, W. Wang, R. Li, Y. Sun, F. Shen, S. Qu, and J. Gao, Plasmonic focusing lens based on single-turn nano-pinholes array, Opt. Express 23 (2015) 17883-17891.
[12] R. Ameling, L. Langguth, M. Hentschel, M. Mesch, P. V. Braun, and H. Giessen, Cavity-enhanced localized plasmon resonance sensing, Appl. Phys. Lett. 97 (2010) 253116.
[13] W. Wang, Z. Guo, R. Li, J. Zhang, Y. Li, Y. Liu and S. Qu, Plasmonics metalens independent from the incident polarizations, Opt. Express 23 (2015) 16782–16791.
[14] O. Krasnykov, A. Karabchevsky, A. Shalabney, M. Auslender, and I. Abdulhalim, Sensor with increased sensitivity based on enhanced optical transmission in the infrared, Opt. Commun. 284 (2011) 1435-1438.
[15] W. Yue, Z. Wang, Y. Yang, J. Li, Y. Wu, L. Chen, B. Ooi, X. Wang, X. Zhang, Enhanced extraordinary optical transmission (EOT) through arrays of bridged nanohole pairs and their sensing applications, Nanoscale 6 (2014) 7917-7923.
[16] K. M. Mayer, and J. H. Hafner, Localized surface plasmon resonance sensors, Chem. Rev. 111 (2011) 3828-3857.

[17] J. Homola, S. S. Yee, and G. Gauglitz, Surface plasmon resonance sensors: review, Sensors and Actuators B: Chemical, 54 (1999) 3-15.
[18] X. Zhang, Z. Li, S. Ye, S. Wu, J. Zhang, L. Cui, ... and B. Yang, Elevated Ag nanohole arrays for high performance plasmonic sensors based on extraordinary optical transmission, J Mater Chem. 22 (2012) 8903-8910.
[19] L. Luo, C. Xie, B. Nie, L. Zeng, Surface Plasmon Resonance Enhanced Highly Efficient Planar Silicon Solar Cell with Au Nanoparticles Decorated Graphene Transparent Electrode, Nano Energy 9 (2014) 112-120.
[20] Z. Jakšic, D.Vasiljevic-Radovic, and M. Sarajlic, "Analyte-targeted patterning of subwavelength aperture arrays with extraordinary optical transmission for enhanced biosensing," In Proc. 8th Int. Conf. on Fundamental and Applied Aspects of Physical Chemistry (Belgrade,2006), pp. 528-30.
[21] L. Luo, W. Xie, Y. Zou, Y. Yu, F. Liang, Z. Huang and K. Zhou, Surface plasmon propelled high-performance CdSe nanoribbons photodetector, Opt. Express 23 (2015) 12979-12988.
[22] K. L. Lee, J. B. Huang, J. W. Chang, S. H. Wu, and P. K. Wei, Ultrasensitive Biosensors Using Enhanced Fano Resonances in Capped Gold Nanoslit Arrays, Sci Rep. 5 (2015) 8547.
[23] Y. Wang , C. Ge, Y. Zou, R. Lu, D. Wang, L. Wang, C. Wu, L. Luo, Plasmonic In nanoparticles induced high-performance photoswitch for blue light detection, Adv. Opt. Mater. 4 (2016) 291-296.
[24] M. Ambati, S. H. Nam, E. Ulin-Avila, D. A. Genov, G. Bartal, and X. Zhang, Observation of stimulated emission of surface plasmon polaritons, Nano Lett. 8 (2008) 3998-4001.
[25] A. D. Luca, M. P. Grzelczak, I. Pastoriza-Santos, L. M. Liz-Marzañ, M. L. Deda, M. Striccoli, and G. Strangi, Dispersed and encapsulated gain medium in plasmonic nanoparticles: a multipronged approach to mitigate optical losses, *ACS* nano 5 (2011) 5823-5829.
[26] W. Zhu, D. Sikdar, F. Xiao, M. Kang, and M. Premaratne, Gold nanoparticles with gain-assisted coating for ultra-sensitive biomedical sensing, Plasmonics 10 (2014) 881-886.
[27] Y. Tao, Z. Guo, A. Zhang, J. Zhang, B. Wang, and S. Qu, Gold nanoshells with gain-assisted silica core for ultra-sensitive bio-molecular sensors, Opt. Commun. 349 (2015) 193-197.
[28] Y. Tao, Z. Guo, Y. Sun, F. Shen, X. Mao, W. Wang, Y. Li, Y. Liu, X. Wang and S. Qu, Sliver spherical nanoshells coated gain-assisted ellipsoidal silica core for low-threshold surface plasmon amplification, Opt. Commun. 355 (2015) 580-585.
[29] Z. G. Dong, H. Liu, J. X. Cao, T. Li, S. M. Wang, S. N. Zhu, and X. Zhang, Enhanced sensing performance by the plasmonic analog of electromagnetically induced transparency in active metamaterials, Appl. Phys. Lett. 97 (2010) 114101.
[30] B. Brian, B. Sepúlveda, Y. Alaverdyan, L. M. Lechuga, and M. Käll, Sensitivity enhancement of nanoplasmonic sensors in low refractive index substrates, Opt. Express 17 (2009) 2015-2023.
[31] X. Zhang, Z. Li, S. Ye, S. Wu, J. Zhang , L. Cui, L. Anran, T. Wang, S. Li, and B. Yang, Elevated Ag nanohole arrays for high performance plasmonic sensors based on extraordinary optical transmission, J. Mater. Chem. 22 (2012) 8903-8910.
[32] S. A. Maier, Plasmonics: fundamentals and applications, Springer Science & Business Media (2007).
[33] Y. Ding, J. Yoon, M. H. Javed, S. H. Song, and R. Magnusson, Mapping surface-plasmon polaritons and cavity modes in extraordinary optical transmission, IEEE Photonics L. 3 (2011) 365-374.
[34] R. Gordon, Light in a subwavelength slit in a metal: Propagation and reflection, Phys. Rev. B 73 (2006) 153405.
[35] J. He, J. Wang, P. Ding, C. Fan, and E. Liang, Gain-assisted plasmon induced transparency in T-shaped metamaterials for slow light, J. Opt. 17 (2015) 055002.
[36] L. J. Sherry, S. H. Chang, G. C. Schatz, R. P. Van Duyne, B. J. Wiley, and Y. Xia, Localized surface plasmon resonance spectroscopy of single silver nanocubes, Nano Lett. 5 (2005) 2034-2038.
[37] N. Liu, M. Mesch, T. Weiss, M. Hentschel, and H. Giessen, Infrared perfect absorber and its application as plasmonic sensor, Nano Lett. 10 (2010) 2342-2348.
[38] L. Meng, D. Zhao, Z. Ruan, Q. Li, Y. Yang, and M. Qiu, Optimized grating as an ultra-narrow band absorber or plasmonic sensor, Opt. Lett. 39 (2014) 1137-1140.
[39] G. Li, Y. Shen, G. Xiao, and C. Jin, Double-layered metal grating for high-performance refractive index sensing, Opt. Express 23 (2015) 8995-9003.